Available on CMS information server

CMS NOTE 2006/029

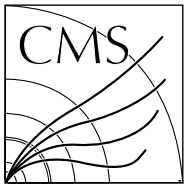

The Compact Muon Solenoid Experiment

CMS Note

Mailing address: CMS CERN, CH-1211 GENEVA 23, Switzerland

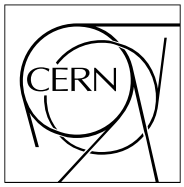

January 31, 2006

Impact of CMS Silicon Tracker Misalignment on Track and Vertex Reconstruction

P. Vanlaer

Interuniversity Institute for High Energies (IIHE), Université Libre de Bruxelles, Bruxelles, Belgium

L. Barbone, N. De Filippis

Istituto Nazionale di Fisica Nucleare (INFN), Bari, Italy

T. Speer

Physik-Institut, Universität Zürich, Zürich, Switzerland

O. Buchmüller, F.-P. Schilling

Physics Department, CERN, Geneva, Switzerland

CMS Collaboration

Abstract

The impact of misalignment on the performance of the CMS silicon tracking devices Pixel and silicon Strip tracker is studied. Misalignment scenarios are used which are expected to resemble the tracker configuration at the LHC start-up as well as after a full track based alignment. The impact of misalignment on general track properties as well as on primary vertexing and vertex fitting is investigated using various event samples.

1 Introduction

The displacement of silicon sensors from their expected positions in the CMS tracker is one of the largest potential sources of tracking uncertainties. In order to study the impact of tracker misalignment on track and vertex reconstruction in concrete physics analysis channels, as well as to study track-based alignment algorithms, a realistic model of misalignment effects has been implemented within the standard CMS software.

The displacement of detector modules is implemented after detector simulation [1] at the reconstruction level [2] using a dedicated software tool [3], which is able to move and rotate all tracker parts (individual modules as well as rods, layers, half-barrels etc.). Hits on tracker sensors are generated according to the ideal detector geometry, and the geometrical shift and rotation of the sensor is introduced afterwards. To achieve a reasonable χ^2 distribution in the track fit, the hit position error is increased by adding an additional error in quadrature, which reflects the size of the assumed misalignment (alignment position error) [3].

Two different default *misalignment scenarios* have been developed, which are explained in detail in [3]. The *Short-Term* (or *First Data Taking*) scenario corresponds to the expected misalignment conditions during the first data taking up to a few hundred pb^{-1}, whereas the *Long-Term* scenario corresponds to the expected level of misalignment after the first full track-based alignment has been carried out:

- **Short-Term (or First Data Taking) scenario:** This scenario is supposed to resemble the expected conditions during the first data taking of CMS (few 100 pb^{-1} of accumulated luminosity). It assumes the availability of the CMS Laser Alignment System [4] for the alignment of the larger structures of the Strip tracker, that the Pixel detector has been aligned to a reasonable level using tracks, and that survey results from the tracker construction, e.g. from photogrammetry, are available. It is further assumed that no track-based alignment of silicon Strip detectors is possible, due to lack of statistics for high p_T tracks. Based on the experience from other experiments, the track-based alignment of the Pixel detector would have reduced its placement uncertainties by one order of magnitude.
- **Long-Term scenario:** It is assumed that after the first few fb^{-1} of data have been accumulated, a first complete track-based alignment down to the sensor level has been carried out, resulting in an overall alignment uncertainty of the Strip tracker of $\sim 20\ \mu\mathrm{m}$.

In this note, a compilation of results which demonstrate the impact of misalignment on track and vertex reconstruction is presented. They have been obtained from the application of the two misalignment scenarios to the CMS silicon tracker. The restriction to the silicon tracker limits the scope of these results to cases where additional constraints from the muon detectors are negligible. This is especially the case for aspects related to B-physics and vertexing in general. Therefore, the largest fraction of results is devoted to these subjects. A study of the impact of misalignment of the CMS muon detectors on muon track reconstruction is presented in [5].

In section 2 the effect of a misaligned tracker on the track reconstruction efficiency, rate of fake tracks and precision of the reconstructed track parameters is presented. The impact on primary vertex reconstruction is discussed in section 3. The effect on the fit parameters of vertices from different physics channels is studied in section 4. Finally, the possible degradation of the invariant mass resolution for the $B_s^0 \to \mu^+\mu^-$ decay is studied in section 5.

2 Impact of Misalignment on General Track Properties

The impact of misalignment of the CMS tracker on general track properties is studied using muons with a given fixed transverse momentum p_T, or in a range of p_T. The event samples are simulated with or without low-luminosity pileup. The effect on the di-lepton invariant mass for muons originating from the $H^0(300\ \mathrm{GeV/c^2}) \to Z^0Z^0 \to e^+e^-\mu^+\mu^-$ decay is also studied.

Tracks are reconstructed using the default CMS *Combinatorial Track Finder* [6] algorithm. The track reconstruction efficiency and track parameter resolutions are defined as in [6, 7] to allow for the comparison of results in the case of perfect alignment. Simulated and reconstructed tracks are associated using links between the simulated and reconstructed hits. For the track finding efficiency determination, a reconstructed track is required to share at least half of its hits with the simulated track. The resolution of a track parameter is defined as the RMS of a Gaussian function fitted to the distribution of the difference between the reconstructed and the simulated values (i.e. the distribution of residuals). During track reconstruction, the alignment position error is accounted for in the search for compatible hits and in the track fitting, by adding it in quadrature to the error matrix of the measured hit position.

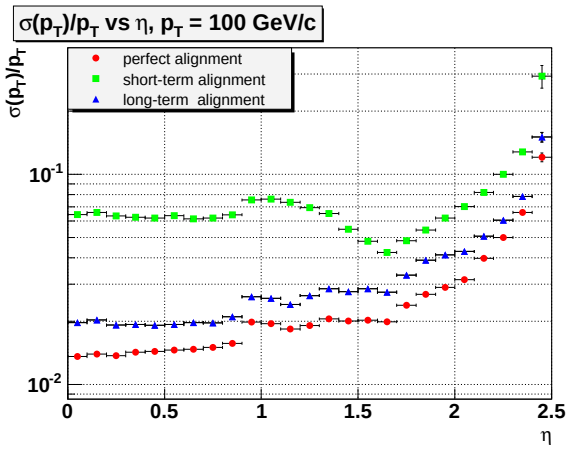

Figure 1: Transverse momentum resolution, divided by p_T, as a function of $|\eta|$ for single muons with $p_T = 100\ \mathrm{GeV}/c$, shown for perfect alignment (red circles) as well as for the short-term (green boxes) and long-term (blue triangles) misalignment scenarios.

2.1 Misalignment Studies Using Single Muon Events

In the following studies, as a benchmark muons with $p_T = 100\ \mathrm{GeV}/c$ are used, which lies in a p_T range relevant for many LHC physics channels of interest. In addition, the chosen p_T value is high enough so that the resolution of the track parameters is not strongly affected by multiple scattering.

The main misalignment effect is a degradation of the resolution of the five track parameters p_T, ϕ, $\cot\theta$, d_0 and z_0, the latter two being defined at the point of closest approach of the track to the beam axis (this point is called the impact point). The transverse and longitudinal impact parameters d_0 and z_0 are the cylindrical coordinates of the impact point ($d_0 = y_0 * cos\phi - x_0 * sin\phi$, where x_0 and y_0 are the transverse coordinates of the impact point). The angle ϕ is the azimuthal angle of the momentum vector of the track at the impact point, and θ is the polar angle.

The dependence of the p_T resolution on the pseudo-rapidity is shown in Fig. 1 for perfect alignment as well as for the short-term and long-term misalignment scenarios, using muons distributed uniformly in $|\eta| < 2.5$. In the case of perfect alignment, the resolution is in good agreement with previous studies [6]: $1.5 - 2\%$ up to a pseudo-rapidity of $|\eta| = 1.7$, while for higher values of $|\eta|$ the lever arm of the measurement is reduced and the resolution is degraded. In the first data taking scenario the resolution is worse by a factor 3 to 4. This degradation is consistent with the precision of the reconstructed hits if the contribution of the detector misalignments is accounted for.

The resolutions of the other track parameters as a function of $|\eta|$ are presented in Figs. 2-5. The d_0 resolution (Fig. 2) is fairly constant with $|\eta|$ with a value of around 9, 35 and 20 μm in the case of perfect alignment, short-term and long-term misalignment scenarios, respectively. In the long-term scenario, the pixel hit resolution dominates, while in the short-term scenario, the large misalignments of the silicon strip tracker in the $R\phi$ projection further degrade the d_0 resolution. Since the z-resolution of the silicon strip detectors is at best around 1 mm (in double-sided layers), the z_0 resolution of high momentum tracks is dominated by the resolution of the pixel hits in all misalignment scenarios, as shown in Fig. 3. The improvement of the z_0 resolution with increasing $|\eta|$ up to $|\eta| = 0.5$ is a known effect. It is due to the fact that in the barrel, as the angle at which the tracks cross the pixel layers increases, the clusters become wider, allowing charge interpolation and improving the pixel-hit resolution [6, 7]. Finally, the resolutions in ϕ and $\cot\theta$ are presented in Figs. 4 and 5. The mean values and the RMS of the residual distributions of the track parameters for the three scenarios are summarized in Tab. 1.

The effect of misalignment on the track reconstruction efficiency is strongly dependent on the value of the alignment position error that is combined with the hit resolution during track finding and fitting. If the alignment position error corresponds to the size of the applied misalignment, full track finding efficiency is recovered, as shown in Fig. 6. The rate of fake tracks however increases from 1.5% to 4.5% due to the fact that a larger number of incorrect hit associations are formed. If the alignment uncertainties are not accounted for, track hits are lost and a significant drop of track finding efficiency is seen in the short-term misalignment scenario. This drop is larger for tracks traversing the TID ($1.2 < |\eta| < 2$), which suffers from comparatively large initial misalignment (since no laser alignment system is available for the TID [3]). The efficiency is recovered at very large $|\eta|$, where the track candidates are extrapolated by a long distance from the pixel disks to the TEC, making the search window for compatible hits wide enough, even without accounting for misalignments. The drop of the efficiency in the

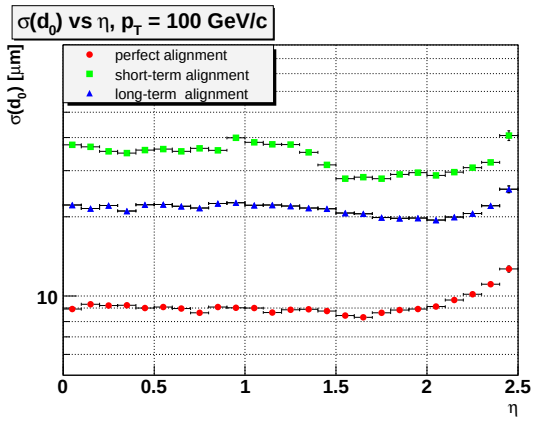

Figure 2: Resolution in the transverse impact parameter d_0 as a function of $|\eta|$ for single muons with $p_T = 100$ GeV/c, shown for perfect alignment (red circles) as well as for the short-term (green boxes) and long-term (blue triangles) misalignment scenarios.

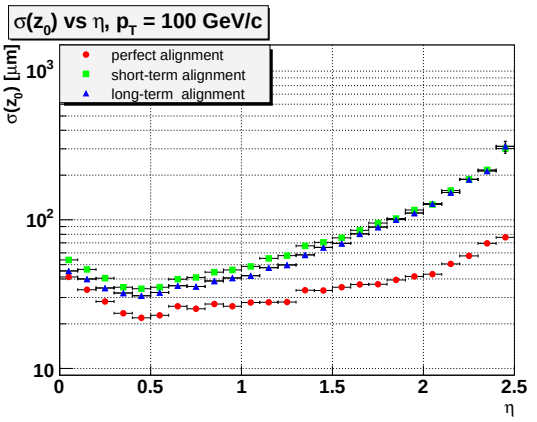

Figure 3: Resolution in the longitudinal impact parameter z_0 as a function of $|\eta|$ for single muons with $p_T = 100$ GeV/c, shown for perfect alignment (red circles) as well as for the short-term (green boxes) and long-term (blue triangles) misalignment scenarios.

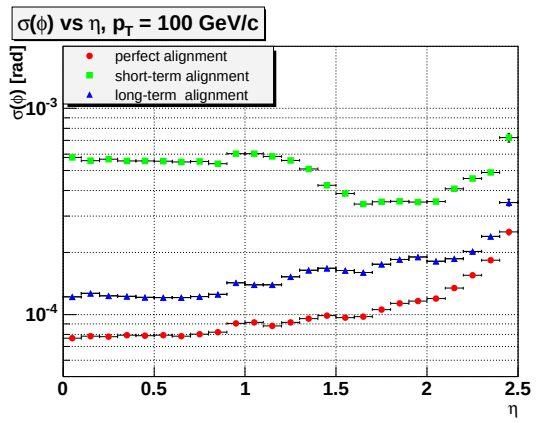

Figure 4: Resolution in ϕ as a function of $|\eta|$ for single muons with $p_T = 100$ GeV/c, shown for perfect alignment (red circles) as well as for the short-term (green boxes) and long-term (blue triangles) misalignment scenarios.

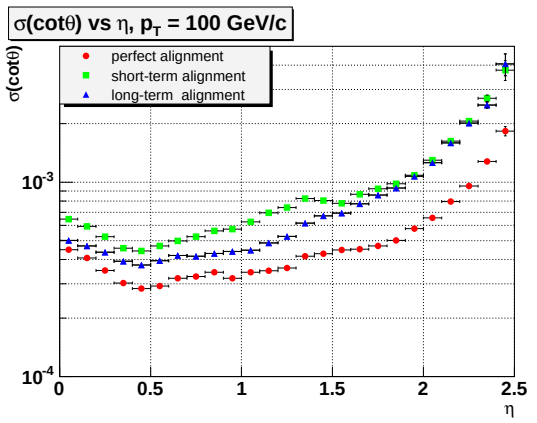

Figure 5: Resolution in $\cot\theta$ as a function of $|\eta|$ for single muons with $p_T = 100$ GeV/c, shown for perfect alignment (red circles) as well as for the short-term (green boxes) and long-term (blue triangles) misalignment scenarios.

region around $\eta \sim 0$ is a known effect [6] due to the gaps between the pixel barrel sensors, which are aligned every 6.4 cm and in particular at $z = 0$, and which cause some tracks not to have the two required pixel hits. At high pseudo-rapidity, the lack of coverage of the two pairs of forward/backward pixel disks causes a slow drop of the efficiency.

The distribution of the reduced χ^2 of the track fit in the case of perfect alignment scenario as well as for the short-term and long-term misalignment scenarios is shown in Fig. 7. In the misalignment scenarios the χ^2 distribution is shifted towards larger values with respect to the ideal tracker geometry. The increase is however moderate, indicating that the alignment error was correctly accounted for during the track fit.

2.2 Misalignment Studies Using $H^0 \to Z^0Z^0 \to e^+e^-\mu^+\mu^-$ Events

In order to study the impact of misalignment on the reconstruction of muons in a broad range of p_T values (up to 250 GeV/c^2), muons from the $H^0 \to Z^0Z^0 \to e^+e^-\mu^+\mu^-$ decay with $m_{H^0} = 300\,\mathrm{GeV}/c^2$, simulated using

Single muons with $p_T = 100$ GeV/c.					
	p_T [GeV/c]	ϕ [rad]	$\cot\theta$	z_0 [μm]	d_0 [μm]
Perfect tracker alignment					
Mean	-1.4	1.3×10^{-5}	1.4×10^{-6}	-0.2	-0.6
σ	2.1	1.0×10^{-4}	4.4×10^{-4}	34.4	9.4
Short-term tracker alignment					
Mean	-1.2	-2.2×10^{-6}	1.3×10^{-4}	-5.0	2.5
σ	6.8	5.0×10^{-4}	8.1×10^{-4}	69.0	34.8
Long-term tracker alignment					
Mean	-1.5	4.0×10^{-6}	-2.3×10^{-5}	6.6	2.3
σ	2.9	1.6×10^{-4}	6.4×10^{-4}	59.6	22.0

Table 1: Biases and resolutions of the track parameters for single muons with $p_T = 100$ GeV/c.

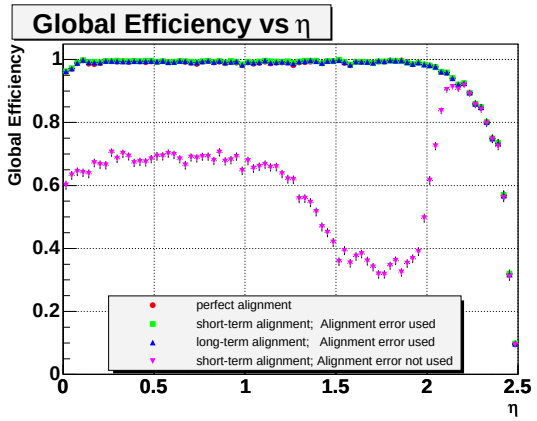

Figure 6: Track finding efficiency as a function of $|\eta|$ for single muons with $p_T = 100$ GeV/c, shown for perfect alignment (red circles), as well as for the short-term and long-term misalignment scenarios when accounting for the alignment uncertainty during track reconstruction (green boxes and blue triangles), and for the short-term scenario without accounting for the alignment uncertainty (purple triangles).

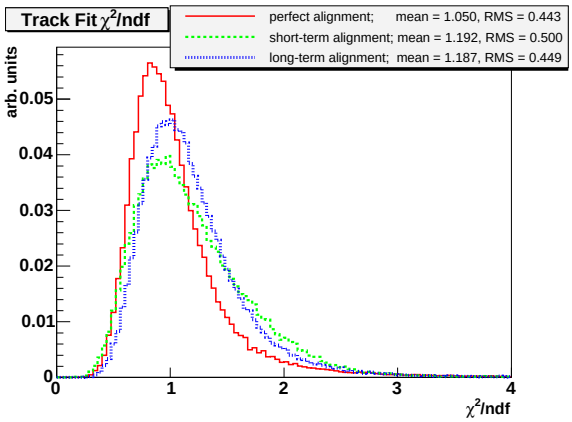

Figure 7: Distributions of the χ^2 per degree of freedom of the track fit for single muons with $p_T = 100$ GeV/c, shown for perfect alignment (red solid) as well as for the short-term (green dashed) and long-term (blue dotted) misalignment scenarios.

low luminosity pile-up, are studied. The p_T resolution as a function of p_T is shown in Fig. 8 for the three scenarios. The effect of misalignment is visible for $p_T > 10$ GeV/c^2 and increases with increasing p_T. Below 10 GeV/c^2 the p_T resolution is dominated by the contribution from multiple scattering. The track finding efficiency is constant with p_T and it is not affected by the misalignment if the alignment position error is taken into account. The mean and RMS values of the distributions of the track parameter residuals are listed in Tab. 2 for the three scenarios.

The distribution of the dimuon invariant mass is also derived from the reconstructed tracks in the three scenarios investigated, as shown in Fig. 9. Misalignment enlarges the width of the Z^0 mass peak by 10% in the short-term scenario with respect to the ideal tracker geometry.

3 Impact of Misalignment on Primary Vertexing

In this section, the effect of tracker misalignment on the primary vertex finding is studied for three physics channels with very different kinematics at the primary vertex: $B_s \to J/\psi\phi$, $t\bar{t}H$ associated Higgs-production, and Drell-Yan (DY) $\mu^+\mu^-$ production with $\sqrt{s} = 115$ GeV/c^2. Vertex finding is performed using the CMS standard Primary Vertex Finder [2], configured with default parameter values.

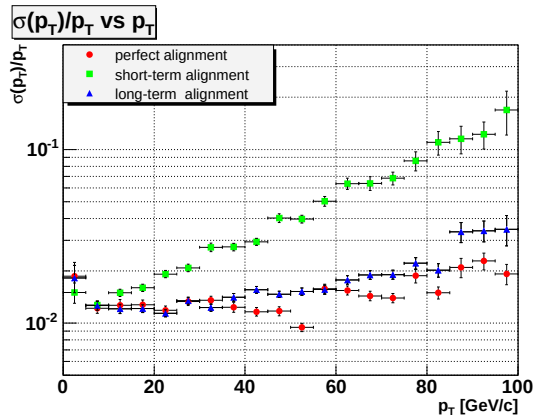

Figure 8: Transverse momentum resolution, divided by p_T, as a function of p_T for muons from $H^0 \to Z^0 Z^0 \to e^+e^-\mu^+\mu^-$ decays with $m_H = 300\,\mathrm{GeV}/c^2$, simulated using low luminosity pile-up, for perfect alignment (red circles) as well as for the short-term (green boxes) and long-term (blue triangles) misalignment scenarios.

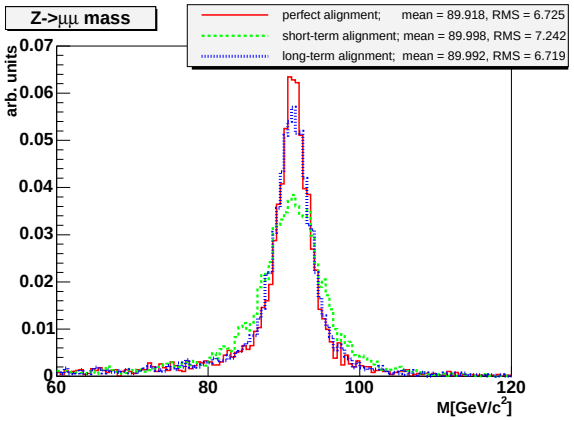

Figure 9: Dimuon invariant mass distribution for muons from $H^0 \to Z^0 Z^0 \to e^+e^-\mu^+\mu^-$ decays with $m_H = 300\,\mathrm{GeV}/c^2$, simulated using low luminosity pile-up, for perfect alignment (red solid) as well as for the short-term (green dashed) and long-term (blue dotted) misalignment scenarios.

Muons from $H^0 \to Z^0 Z^0 \to e^+e^-\mu^+\mu^-$					
	p_T [GeV/c]	ϕ [rad]	$\cot\theta$	z_0 [μm]	d_0 [μm]
Perfect tracker alignment					
Mean	0.1	-3.0×10^{-6}	-2.8×10^{-7}	0.3	0.4
σ	0.7	1.3×10^{-4}	4.1×10^{-4}	31.4	10.9
Short-term tracker alignment					
Mean	0.1	-1.6×10^{-5}	1.6×10^{-4}	-8.2	3.6
σ	2.3	5.3×10^{-4}	7.4×10^{-4}	59.1	36.6
Long-term tracker alignment					
Mean	0.1	-1.5×10^{-5}	-7.0×10^{-6}	4.7	3.8
σ	0.8	1.8×10^{-4}	5.8×10^{-4}	51.0	24.3

Table 2: Biases and resolutions of the track parameters for muons from $H^0 \to Z^0 Z^0 \to e^+e^-\mu^+\mu^-$.

3.1 Description of the Primary Vertex Finding Algorithm

The standard Primary Vertex Finder performs a global primary vertex reconstruction, starting from all reconstructed tracks available in the event. It proceeds in 4 steps:

1. An initial track selection is performed to reject secondary tracks, and to reduce computation time. The selection criteria are:
   - the significance of the transverse impact parameter $d_0/\sigma(d_0)$ is required to be smaller than a configurable value, 3 by default;
   - the track p_T is required to be larger than a configurable value, 1.5 GeV/c by default.
2. Tracks are extrapolated to the beam line $(x = 0; y = 0)$, and grouped according to their separation in z, in order to form primary vertex candidates. The maximum separation between two successive tracks belonging to the same primary vertex candidate is configurable. The default value is 1 mm.
3. Each primary vertex candidate is then fit, and tracks incompatible with the vertex are discarded recursively, starting from the track with worst compatibility. Track removal stops when all tracks are compatible to more than P percent ($P = 5\%$ by default).

Channel	Multiplicity of rec. tracks		ϵ
	from primary vertex	$p_T > 1.5$ GeV/c	
Perfect tracker alignment			
$B_s^0 \to J/\psi\phi$	12.4	4.4	0.835 ± 0.005
$t\bar{t}H$	35	20	0.993 ± 0.001
DY	21.7	9.4	0.940 ± 0.004
Short-term tracker alignment			
$B_s^0 \to J/\psi\phi$	12.9	4.6	0.825 ± 0.005
$t\bar{t}H$	33	19	0.958 ± 0.003
DY	21.7	9.4	0.914 ± 0.004
Long-term tracker alignment			
$B_s^0 \to J/\psi\phi$	12.4	4.4	0.826 ± 0.005
$t\bar{t}H$	35	20	0.960 ± 0.004
DY	21.7	9.4	0.916 ± 0.004

Table 3: Multiplicity of reconstructed tracks from the signal primary vertex, before and after the track selection cut $p_T > 1.5$ GeV/c, and vertex finding efficiency ϵ for the signal primary vertex.

4. A final cleaning of the vertex candidates is made. Vertices with a χ^2_{fit} probability below a given value are rejected ($P(\chi^2_{fit}) > 1\%$ by default). Vertices compatible with $(x = 0; y = 0)$ to less than Q percent are rejected ($Q = 1\%$ by default).

All the compatibility probabilities are computed assuming Gaussian resolutions. The compatibility with the beam axis is computed accounting for a Gaussian beam spot with a width of 15 μm in x and y.

Eventually, the reconstructed primary vertices are sorted and returned in decreasing order of "hardness". The sorting criterion used is $\sum_{i=1}^{N_{tracks}} (p_T^i)^2$. In most physics cases, the ordering is such that the first vertex in the list is the vertex of the signal event. However in specific physics cases, e.g. when the signal vertex is soft and has a low multiplicity, the other vertices also have to be considered as possible signal vertices.

3.2 Analysis

We characterize the algorithm performance with the following quantities:

- The vertex finding efficiency ϵ, defined as the efficiency to find any of the primary vertex candidates within $\Delta z = 500$ μm of the simulated signal vertex;
- For the primary vertex candidate nearest to the simulated signal vertex within that interval, we compute:
  - the position resolutions $\sigma_{x,y,z}$, defined here as the standard deviation of a Gaussian fit to the distributions of the residuals with respect to the simulated vertex position in x, y and z;
  - the bias, i.e. the average value of these distributions;
  - the tails, defined as the 95% coverage of the residual distributions. For a Gaussian distribution, this coverage corresponds to two standard deviations. The fraction of events in the tails can then be evaluated by comparing the 95% coverage to $2 \times \sigma_{x,y,z}$.
  - the precision of the fit covariance matrix, evaluated by the standard deviations of a Gaussian fit to the distributions of the standardized residuals in x, y and z. These standard deviations are further called *pulls* and noted $Pull_{x,y,z}$. The standardized residuals are well described by a single Gaussian distribution.

3.3 Event Samples

The multiplicities of reconstructed tracks from the primary vertex, before and after the track selection cut of $p_T > 1.5$ GeV/c, are summarized in Tab. 3 for the three channels studied. The primary vertex in the $B_s \to J/\psi\phi$ sample is soft, with 12.4 reconstructed tracks per vertex (4.4 with a p_T above 1.5 GeV/c). The $t\bar{t}H$ and DY events are harder and have larger track multiplicities.

X- and Y-coordinates					
Channel	$\sigma_{x,y}$ [μm]	95% Cov. [μm]	Bias [μm] X	Bias [μm] Y	$Pull_{x,y}$
Perfect tracker alignment					
$B_s^0 \to J/\psi\phi$	45	119	-0.5 ± 0.6	-0.6 ± 0.6	1.15
$t\bar{t}H$	10	26	-0.0 ± 0.2	0.1 ± 0.2	1.16
DY	13.5	46	0.2 ± 0.3	-0.5 ± 0.3	1.12
Short-term tracker alignment					
$B_s^0 \to J/\psi\phi$	51	128	-5.8 ± 0.7	12 ± 0.7	1.16
$t\bar{t}H$	18	47	2.4 ± 0.2	16 ± 0.2	1.48
DY	24	62	1.6 ± 0.4	16 ± 0.4	1.23
Long-term tracker alignment					
$B_s^0 \to J/\psi\phi$	51	127	-10 ± 0.7	11 ± 0.7	1.16
$t\bar{t}H$	17	47	-9.5 ± 0.4	11 ± 0.4	1.46
DY	22	59	-8.9 ± 0.4	11 ± 0.4	1.28

Table 4: Primary vertex finding resolutions, fraction of tails, biases and pulls (x and y coordinates).

The samples are simulated with low luminosity (2×10^{33} cm^{-2}s^{-1}) pile-up. Both short-term and long-term alignment scenarios have been simulated. Among the misalignment parameters, the residual systematic shifts of the pixel half-barrels have the largest effects on the primary vertices, as will be shown further. In the alignment scenarios simulated, these shifts $(\Delta x, \Delta y, \Delta z)$ amount to (-1.6, -9.2, 7.5) μm for the $+x$ half-barrel, and (23.9, -11.8, -0.7) μm for the $-x$ half-barrel. Both scenarios assume the same misalignment, since the pixel detector is supposed to be alignable within a few days using tracks.

3.4 Vertex Finding Efficiency

The vertex finding efficiencies in the three misalignment scenarios are given in Tab. 3 for the three channels studied. The effect of tracker misalignment on the primary vertex finding efficiency is small. A maximum drop of 3.5% is observed among the samples studied. The reason for this drop is the larger fraction of vertices failing the selection cut on the compatibility with the beam axis. A selection criterion which is more robust against non-Gaussian tails in the vertex resolution thus seems advisable. It should be noted that the vertex finding efficiency for soft physics can be increased by lowering the track p_T cut. In the $B_s^0 \to J/\psi\phi$ channel, with a p_T cut at 0.7 GeV/c, the vertex finding efficiency increases to (96.3 ± 0.3)%. The position resolutions also improve, from 45 μm to 37 μm in x and y, and from 64 μm to 48 μm in z, for the $B_s^0 \to J/\psi\phi$ channel.

3.5 Resolutions, Tails, Biases and Pulls

The resolutions, fraction of tails, biases and pull widths are summarized in Tabs. 4 and 5. The position resolution is significantly affected, as expected. In the long-term misalignment scenario, the primary vertex biases in the three coordinates are consistent with the residual shifts of the pixel half-barrels $(\Delta x, \Delta y, \Delta z)$: the innermost track hits are thought to be located at a position $-(\Delta x, \Delta y, \Delta z)$ away from their true position, and since about half of the tracks cross each half-barrel, the observed biases are approximately the mean of the residual shifts of the two half-barrels. This was cross-checked by separating the vertices in two categories, one with a majority of tracks crossing the $(+x)$ half-barrel, and the other with a majority of tracks crossing the $(-x)$ half-barrel. The primary vertex biases for the two categories become (-7.7, 10.8, -8.3) μm and (-13.2, 10.4, -8.7) μm respectively, in the $B_s^0 \to J/\psi\phi$ sample. As expected, the shift of the $(+x)$ half-barrel has thus a larger effect on the first category, while the shift of the $(-x)$ half-barrel affects more the second category. In the short-term scenario, the misalignment of the silicon strip tracker is ten times worse, which further affects the primary vertex bias. The effect is larger for harder events, since the constraint on high-momentum tracks from hits in the silicon strip tracker is stronger (less multiple scattering).

The worsening of the primary vertex resolution is of the same order of magnitude for soft and hard events (6-8 μm in absolute value). Misalignments effects thus do not add up in quadrature with the resolutions obtained in the perfect alignment case. This indicates that a large fraction of the degradation comes from different systematic shifts of different detector parts, giving rise to several track populations with different biases.

The distributions of residuals and pulls in x and z for the $B_s^0 \to J/\psi\phi$ and $t\bar{t}H$ samples are shown for the case of

Z-coordinate				
Channel	σ_z [μm]	95% Cov. [μm]	Bias [μm]	$Pull_z$
Perfect tracker alignment				
$B_s^0 \to J/\psi\phi$	64	229	-2.7 ± 0.9	1.15
$t\bar{t}H$	14	36	-0.5 ± 0.3	1.12
DY	25	76	-0.3 ± 0.5	1.14
Short-term tracker alignment				
$B_s^0 \to J/\psi\phi$	67	235	-2.6 ± 0.7	1.28
$t\bar{t}H$	22	66	3.6 ± 0.2	1.41
DY	35	93	3.7 ± 0.5	1.19
Long-term tracker alignment				
$B_s^0 \to J/\psi\phi$	67	242	-7.8 ± 0.7	1.29
$t\bar{t}H$	21	58	-4.1 ± 0.5	1.38
DY	33	92	-4.7 ± 0.5	1.23

Table 5: Primary vertex finding resolutions, fraction of tails, biases and pulls (z coordinate).

perfect alignment in Figs. 10 and 11, respectively.

4 Impact of Misalignment on Vertex Fitting

In order to evaluate the impact of misalignment on the fit of the vertices themselves, the reconstruction of vertices is evaluated using only tracks matched to the simulated tracks which were produced in the selected decay, without applying any cuts. As such, only mis-measured tracks are included in the fit, without contamination from tracks originating from another vertex. In addition to the already described primary vertices of the $B_s^0 \to J/\psi\,\phi$ and $t\bar{t}H$ channels, the secondary vertex of the decay $B_s^0 \to J/\psi\,\phi$ is also studied, since a precise determination of the decay position is essential for both the selection and the measurement of the physics parameters of interest. In that vertex, four tracks with relatively low p_T are fitted to a vertex. These tracks are usually selected by kinematic requirements, and do not rely on a vertex finding technique as used for the primary vertex[1)].

The vertices are fitted with the well-known Kalman Filter [8]. The use of adaptive filters and their robustness with respect to tracker misalignment is studied in a forthcoming note [9]. For the evaluation of the results, the same variables are used as in section 3. Obviously, no efficiency can be defined in this context, as only the correct tracks are used.

For each sample, the main properties of the fits are summarized in Tabs. 6 and 7. For the primary vertices, the resolutions are similar to those obtained by the primary vertex finder, albeit with larger coverage, indicating an increase of the tails of the distributions. It could be argued that the resolution and tails of the Kalman fitter should be better than the primary vertex finder, since no track from another vertex is included in the fit. Our results indicate that the primary vertex finder is able to reject mis-measured tracks and tracks from other vertices, hence yielding better results than a vertex fitter alone. On the effect of the misalignment, the conclusions are identical to those drawn for the primary vertex finder study. The misalignment significantly degrades the estimated positions, both in terms of resolution and bias.

5 Impact of Misalignment on $B_s^0 \to \mu^+\mu^-$

CMS has studied [10] the possibility of observing the rare decay $B_s^0 \to \mu^+\mu^-$ ($B.R. \sim 3.5 \times 10^{-9}$) with the CMS detector using full simulation and reconstruction. The means to reject the overwhelming background from direct muons, mainly originating from $b\bar{b}$ pairs produced via gluon splitting, are (1) an invariant mass cut; (2) secondary vertex reconstruction and (3) isolation in both the tracker as well as the calorimeter. The High-level Trigger (HLT) selection strategy for this channel was studied in [11]. Since both the pixel as well as the strip tracker are used at the HLT level to perform the invariant mass reconstruction as well as a loose secondary vertex reconstruction, the impact of tracker misalignment needs to be considered already in the online selection. In the following, the impact of misalignment on the invariant mass reconstruction is studied.

[1)] It should be noted that a cut on the transverse momentum of the muons is placed by the Monte Carlo generator. Only decays where both muons have a p_T above 2 GeV/c are retained.

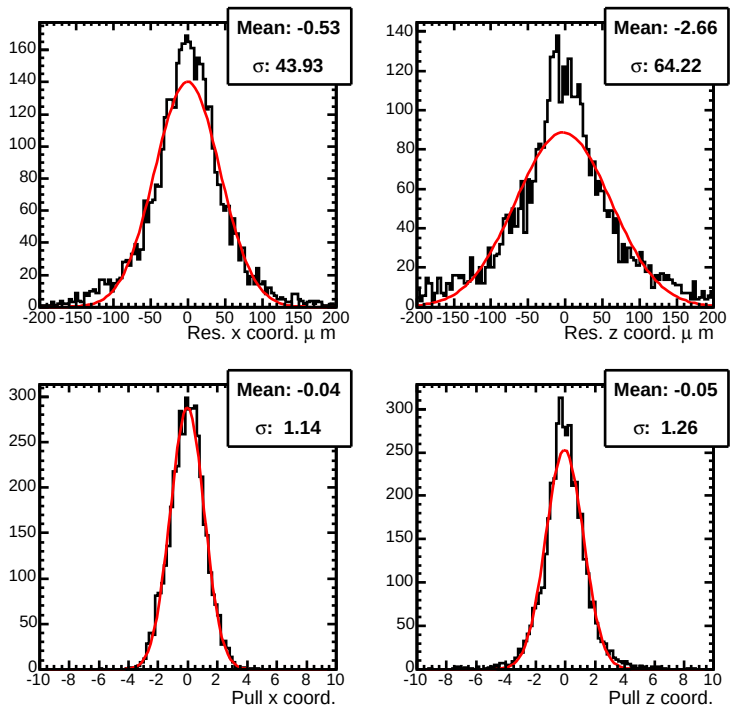

Figure 10: Primary vertex reconstruction: Distributions of residuals (top) and pulls (bottom) in x (left) and z (right), shown for the $B_s^0 \to J/\psi\phi$ sample in the case of perfect tracker alignment. The curves are Gaussians fitted to the distributions.

Channel	Average χ^2/ndf	Average $P(\chi^2)$	Average Time [μs]
Perfect tracker alignment			
$B_s^0 \to J/\psi\,\phi$ (SV)	1.32	0.465	1.29
$B_s^0 \to J/\psi\,\phi$ (PV)	1.29	0.465	3.68
$t\bar{t}H$	2.06	0.207	7.54
Short-term tracker alignment			
$B_s^0 \to J/\psi\,\phi$ (SV)	1.2	0.485	1.39
$B_s^0 \to J/\psi\,\phi$ (PV)	1.38	0.436	3.81
$t\bar{t}H$	2.08	0.182	8.65
Long-term tracker alignment			
$B_s^0 \to J/\psi\,\phi$ (SV)	1.17	0.493	1.4
$B_s^0 \to J/\psi\,\phi$ (PV)	1.27	0.472	3.66
$t\bar{t}H$	1.98	0.222	8

Table 6: Vertex fitting: Main statistical properties of the estimated vertices.

A sample of 1000 $B_s^0 \to \mu^+\mu^-$ signal events has been simulated, digitized and reconstructed using the standard CMS software. Tracks are reconstructed using the standard Combinatorial Track Finder ($p_T > 0.9$ GeV/c). The two tracks (muons) originating from the B_s^0 decay are identified using two different methods: In the first method ('Generator PID'), the two reconstructed muon tracks matching the simulated tracks originating from the B_s decay are selected. In the second method ('Reco PID'), out of the tracks with transverse momentum $p_T > 3$ GeV/c the two with the highest p_T are selected. The invariant mass is then reconstructed from these two tracks.

The invariant mass distribution of the B_s^0 candidate obtained using the 'Generator PID' method is shown in Fig. 12. The solid histogram corresponds to the ideal tracker (no misalignment), the dotted histogram corresponds to a misaligned tracker according to the short-term scenario from [3], and the dashed histogram corresponds to the long-term scenario. The resolutions indicated for each case have been obtained by fitting Gaussians to the mass distributions. For the ideal tracker (no misalignment) the resolution is 46 MeV/c^2. In the case of the short-term scenario, the invariant mass resolution is degraded by $\sim 9\%$, to 50 MeV/c^2. In the case of the long-term scenario,

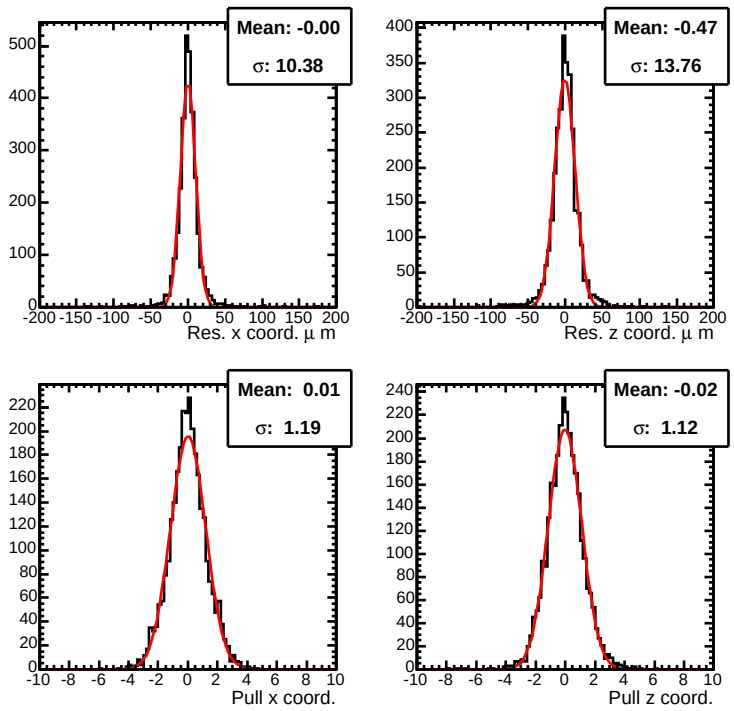

Figure 11: Primary vertex reconstruction: Distributions of residuals (top) and pulls (bottom) in x (left) and z (right), shown for the $t\bar{t}H$ sample in the case of perfect tracker alignment. The curves are Gaussians fitted to the distributions.

Process	x-coordinate				z-coordinate			
	σ_x [μm]	Bias [μm]	95% Cov. [μm]	$Pull_x$	σ_z [μm]	Bias [μm]	95% Cov. [μm]	$Pull_z$
Perfect tracker alignment								
$B_s^0 \to J/\psi\,\phi$ (SV)	54.2	0.545	164	1.09	72.6	-0.718	445	1.08
$B_s^0 \to J/\psi\,\phi$ (PV)	43.8	0.596	176	1.11	54	0.633	223	1.07
$t\bar{t}H$	13.5	-0.299	106	1.45	17.2	-0.0625	116	1.43
Short-term tracker alignment								
$B_s^0 \to J/\psi\,\phi$ (SV)	66.6	-2.5	190	1.12	84	1.82	519	1.08
$B_s^0 \to J/\psi\,\phi$ (PV)	49.5	-8.16	233	1.16	57.7	-2.32	282	1.07
$t\bar{t}H$	24.3	0.69	205	1.97	24.3	1.79	244	1.58
Long-term tracker alignment								
$B_s^0 \to J/\psi\,\phi$ (SV)	63.8	-10.9	177	1.09	80.5	-3.86	502	1.07
$B_s^0 \to J/\psi\,\phi$ (PV)	47.9	-10.8	187	1.13	57.2	-4.86	233	1.06
$t\bar{t}H$	20.9	-11.6	116	1.83	22.3	-4.25	129	1.56

Table 7: Vertex fitting: Main properties of the residual and pull distributions of the estimated vertices.

it recovers to 49 $\mathrm{MeV/c^2}$.

A similar degradation is observed in case of the more realistic 'Reco PID' method, as can be seen in Fig. 13. The corresponding numbers for the invariant mass resolution are 45 $\mathrm{MeV/c^2}$ without misalignment, 54 $\mathrm{MeV/c^2}$ (+20%) for the short-term scenario and 49 $\mathrm{MeV/c^2}$ (+9%) for the long-term scenario.

The observed impact of misalignment on the invariant mass resolution is rather moderate. This is due to the low transverse momentum of the B_s^0 decay muon tracks, where the accuracy of the track reconstruction is largely determined by multiple scattering (included in the simulation), such that the influence of misalignment is a second order effect;

In summary, assuming that the pixel detector can be aligned with an overall precision of 5 to 10 μm using track based alignment from the beginning of data taking already, the impact of misalignment of the strip tracker on the dimuon mass resolution in the decay $B_s^0 \to \mu^+\mu^-$ is of the order of 10 to 20% and thus does not significantly

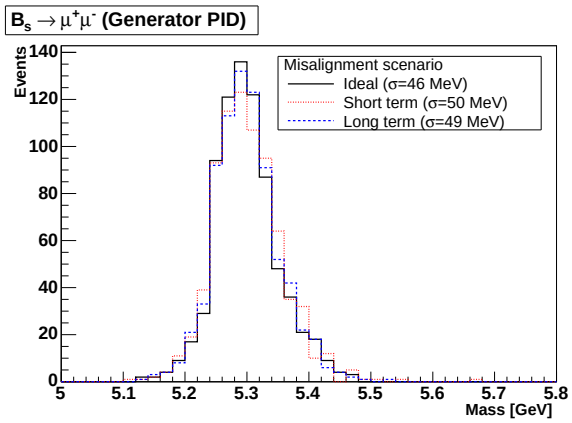

Figure 12: Invariant mass of the B_s^0 candidate reconstructed from tracks associated with the B_s^0 decay at the generator level. The black solid line corresponds to the ideal tracker (no misalignment), whereas the red dotted (blue dashed) line corresponds to a misaligned tracker according to the short-term (long-term) misalignment scenario.

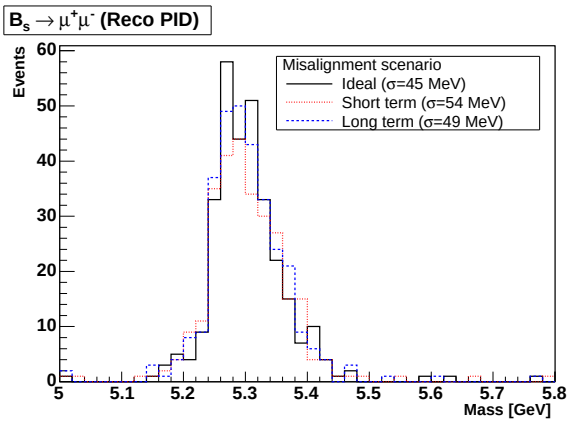

Figure 13: Invariant mass of the B_s^0 candidate reconstructed using the two highest transverse momentum tracks of the event. The black solid line corresponds to the ideal tracker (no misalignment), whereas the red dotted (blue dashed) line corresponds to a misaligned tracker according to the short-term (long-term) misalignment scenario.

deteriorate the CMS performance for this channel for both High-level Trigger as well as offline selection.

6 Conclusions

In conclusion, although the effects of tracker misalignment are clearly visible in the observables studied in this note, within the assumptions made the physics reach of CMS is not dramatically affected due to misalignment. In particular, the charge of a particle can still be measured in the CMS tracker up to transverse momenta of $p_T \sim 1.5\ (5.0)\ \mathrm{GeV/c}$, assuming the short-term (long-term) misalignment scenario.

References

[1] CMS Collaboration, Simulation Software **OSCAR**, `http://cmsdoc.cern.ch/OSCAR/`

[2] CMS Collaboration, Reconstruction Software **ORCA**, `http://cmsdoc.cern.ch/orca/`

[3] I. Belotelov *et al.*, *Simulation of Misalignment Scenarios for CMS Tracking Devices*, **CMS Note 2006/008** (2006).

[4] A. Ostaptchouk, S. Schael, R. Siedling and B. Wittmer, *The Alignment System of the CMS Tracker*, **CMS Note 2001/053** (2001).

[5] F. Matorras *et al.*, *Effect of Misalignment Scenarios on Muon reconstruction*, **CMS Note 2006/017** (2006).

[6] CMS Collaboration, The Trigger and Data Acquisition Project, Volume 2, *Technical Design Report*, **CERN-LHCC-2002/26** (2002) p.265.

[7] CMS Collaboration, The Tracker Project, *Technical Design Report*, **CERN/LHCC 1998-06** (1998); CMS Collaboration, *Addendum to the Tracker TDR*, **CERN/LHCC 2000-16** (2000).

[8] R. Frühwirth, R. Kubinec, W. Mitaroff and M. Regler, *Comp. Phys. Commun.* **96** (1996) 169.

[9] T. Speer *et al.*, *Vertex Fitting in the CMS Tracker*, **CMS Note** in preparation.

[10] A. Nikitenko, A. Starodumov and N. Stepanov, *Observability of $B^0_{(d),s} \to \mu^+\mu^-$ decay with the CMS detector*, **CMS Note 1999/039** (1999). [hep-ph/9907256]

[11] CMS Collaboration, The Trigger and Data Acquisition Project, Volume 2, *Technical Design Report*, **CERN-LHCC-2002/26** (2002) appendix G2.1.